Phosphoproteome Profiling of Mouse Liver During Normal Aging

Jiang-Feng Liu
Chinese Academy of Medical Sciences&Peking Union Medical College
Yue Wu
Nankai University
Ye-Hong Yang
Chinese Academy of Medical Sciences & Peking Union Medical College
Song-Feng Wu
Chinese Academy of Medical Sciences
Shu Liu
Chinese Academy of Medical sciences
Ping Xu (xuping@ncpsb.org.cn)
Chinese Academy of Medical Sciences
Juntao Yang
Chinese Academy of Medical Sciences & Peking Union Medical College

Research Article

Keywords: normal aging, mouse, liver, phosphoproteome, label free

Posted Date: October 27th, 2021

DOI: https://doi.org/10.21203/rs.3.rs-966762/v1

Abstract

Background

Aging is a complex biological process accompanied by a time-dependent functional decline that affects most living organisms. Omics studies help to comprehensively understand the mechanism of aging and discover potential intervention methods. Old mice were frequently obese with a fatty liver.

Methods

We applied mass spectrometry-based phosphoproteomics to obtain a global phosphorylation profile of liver in mice aged 2 or 18 months. A total of 5,685 phosphosites in 2,335 proteins were filtered for quantitative analysis. Phosphoproteome weakly separated young and old mice.

Results

Combining kinase prediction, kinase-substrate interaction analysis, and KEGG functional enrichment analysis, we observed high phosphorylation of fatty acid biosynthesis, b-oxidation, and potential secretory process, together with low phosphorylation of Egfr-Sos1-Araf/Braf-Map2k1-Mapk1 pathway and Ctnnb1 during aging. Proteins with differentially expressed phosphosites seemed more directly related to aging-associated fatty liver phenotype compared to the differentially expressed transcripts. Phosphoproteome may observe distinctive biological functions lost in transcriptome and proteome.

Conclusions

In summary, we constructed a phosphorylation-associated network in the liver of mice during normal aging, which may help to discover novel anti-aging strategies.

Highlights

· The first phosphoproteome profiling of mouse livers during normal aging.

· A total of 5,685 phosphosites in 2,335 proteins were quantified in this study.

· A phosphorylation-regulated pathway network was constructed.

· Metabolism, secretion, and cell cycle might be dysregulated during normal aging.

Introduction

Aging and aging-associated diseases have brought great suffering and economic burden to both individuals and society [1]. Anti-aging interventions have been searched for years and development of modern biology promoted the discovery of anti-aging methods. Hallmarks of aging were summarized as epigenetic alterations, loss of proteostasis, deregulated nutrient sensing, cellular senescence, etc. [2].

Several interventions, including senolytics, NAD precursors, metformin, exercise, caloric restriction, etc., can potentially increase the health span and/or lifespan [3]. However, pivotal anti-aging methods are still deficient because our global view of normal aging is rather incomplete.

Omics analysis offers the advantage of obtaining an overall profile of biological processes and has been applied in aging-associated researches [4]. In this study, we focused on phosphoproteome profiling of mouse liver during normal aging. The liver is the biggest metabolic organ in human and mice. Although aging liver shows relatively modest physiological changes [5], omics studies have discovered some featured molecular alterations, such as remodeled DNA methylation [6], increased inflammation [7, 8], disrupted metabolic homeostasis and circadian metabolism [9]. Phosphoproteome has been used for liver functional research, including circadian control [10], nonalcoholic fatty liver disease and steatohepatitis [11]. Phosphorylation is an economic way for organism to respond to physiological changes and has accumulated abundant research data. As the phosphoproteome profiling of liver during aging has not been investigated, we applied mass spectrometry-based phosphoproteomics to obtain the first global in vivo quantification of aging-associated phosphorylation in mouse livers.

Materials And Methods

1. Animals

Wild-type C57BL/6J male mice were allowed to take food and water ad libitum. The colony rooms were maintained at a constant temperature and humidity with a 12:12 light/dark cycle. All animal protocols were approved by the Animal Care and Use Committee of the Institute of Basic Medical Sciences, Chinese Academy of Medical Sciences and Peking Union Medical College.

2. Sample preparation

Fourteen two-month-old mice were used in the young group and ten eighteen-month-old mice were used in the old group. Mice were euthanized by massive bloodletting from the orbital vessel after anesthesia with tribromoethanol. Next, the whole liver was detached from each mouse, immediately dissected, and stored separately. Samples acquired for phosphoproteome and transcriptome analyses were immediately frozen in liquid nitrogen and transferred to -80 ℃ until use. Samples for H & E and Masson analyses were quickly placed in 4% paraformaldehyde (PFA). Samples for oil red O analysis were appropriately embedded into optimal cutting temperature compound (OCT) and stored at -80 ℃ until use.

3. Morphological analysis

3.1 H & E and Masson staining

Liver samples were fixed in 4% PFA overnight. Fixed tissues were dehydrated by 75% ethanol for 4 h, 85% ethanol for 2 h, 90% ethanol for 2 h, 95% ethanol for 1 h, absolute ethanol for 30 min twice, ethanol-dimethylbenzene for 5 min, and dimethylbenzene twice for 10 min. Dehydrated tissues were embedded in paraffin and cut in 4 mm-thick sections. The paraffin embedded sections were successively placed in

dimethylbenzene twice for 20 min each, absolute ethanol for 10 min twice, 95% ethanol for 5 min, 90% ethanol for 5 min, 80% ethanol for 5 min, 70% ethanol for 5 min, and washed by distilled water.

For H & E staining, hydrated sections were placed in hematoxylin solution for 3-8 min, 1% hydrochloric acid/ethanol differentiation solution for seconds, 0.6% ammonia for seconds, and eosin solution for 1-3 min.

For Masson staining, hydrated sections were processed according to the manufacturer's protocol of the Masson staining kit (Wuhan Goodbio Technology Co., Ltd, G1006).

Stained sections were subsequently transferred into 95% ethanol for 5 min twice, absolute ethanol for 5 min twice, and dimethylbenzene for 5 min twice. Next, the sections were dried and sealed with neural gum. Pictures were taken with a Nikon Eclipse CI imaging system.

3.2 Oil Red O staining

Liver samples embedded in OCT were moved to a freezing microtome and cut into 8 mm-thick sections at -20 ℃. The sections were dried at room temperature for 10 min, fixed with 4% paraformaldehyde (PFA) for 15 min, and washed with phosphate-buffered saline (PBS) for 5 min three times. Sections were transferred into oil red O solution (G1016, Goodbio Technology Co., Ltd) for 10 min, followed by 75% ethanol for 2 s, and then washed with water for 1 min. Next, the sections were transferred to hematoxylin solution for 1 min, 1% hydrochloric acid/ethanol differentiation solution for 3 s, and 0.6% ammonia for 3 s, after which they were washed with water. Excess water was removed, and glycerin gelatin was used to seal the sections. Pictures were taken using a Nikon Eclipse CI imaging system (Japan).

4. Phosphoproteome and analysis

4.1 Protein Extraction and Digestion

Mouse liver tissue samples were ground in liquid nitrogen and sonicated with lysis buffer (9 M Urea, 10 mM Tris–HCl (pH 8.0), 30 mM NaCl, 50 mM IAA, 5 mM $Na_4P_2O_7$, 100 mM Na_2HPO_4 (pH 8.0), 1 mM NaF, 1 mM Na_3VO_4, 1 mM sodium glycerophophate, 1% phosphatase inhibitor cocktail 2 (Sigma, St. Louis, USA), 1% phosphatase inhibitor cocktail 3 (Sigma, St. Louis, USA), 1 tablet of EDTA-free protease inhibitor cocktail (Roche, Basel, Switzerland) for every 10 mL of lysis buffer). Then the total lysate was centrifuged at 17,000 × *g* for 8 min at 4 ℃ to remove debris. The evaluation of protein concentration and subsequent in-gel digestion was performed as previously described [12]. In brief, 1 mg proteins were used as starting material for each sample, the proteins were reduced with 5 mM DTT for 30 min at 45 °C and were alkylated with 20 mM iodoacetamide for 30 min at room temperature in the dark. Next, proteins were resolved on a 10% SDS-PAGE gel and running for a 0.8 cm length and then stained with Coomassie Blue G-250. The entire gel lane was sliced into 1 mm^3 pieces and destained followed by in-gel digestion with 10 ng/μL Trypsin (Promega, Madison, WI, USA) at 37 °C incubation overnight.

4.2 Phosphopeptides Enrichment

Phosphopeptides were enriched by Ti^{4+}-IMAC method [13] as previously reported with minor modifications. Briefly, peptide mixtures were resuspended in 500 μL loading buffer (5% ACN, 50 mM NH_3HCO_3) and acidified with 500 μL binding buffer (80% ACN, 6% TFA) followed by the addition of 30 mg Ti^{4+}-IMAC beads. Then the mixtures were mixed wildly on Vortex Genie2 for 30 min and centrifuged at 17,000 × *g* for 6 min to remove the supernatant. The beads were washed with 1.8 mL wash buffer 1 (80% ACN, 6% TFA) once and 1.8 mL wash buffer 2 (80% ACN, 0.1 TFA) twice and all the wash buffers in each step were removed by centrifugation at 17,000 × *g* for 6 min. Afterwards the beads were resuspended in 1 mL elution buffer (10% $NH_3 \cdot H_2O$) and the mixture was vortexed for 15 min and sonicated in ice water for 15 min followed by centrifugation at 17,000 × *g* for 6 min. The eluted supernatant was collected. The beads were vortexed for 5 min in another 500 μL elution buffer and centrifuged to collect the supernatant. The eluted supernatants were combined and centrifuged at 21,000 × *g* for 8 min to further remove the beads. Then the supernatant was vacuum dried and the eluted phosphopeptides were stored at -80 ℃.

4.3 Stage-Tip Separation

The homemade C18 Stage-Tip [14] was used to separate the phosphopeptides in 3 fractions. The Stage-Tip was firstly activated with 40 μL methanol, then washed with 40 μL wash buffer (80% ACN in 10% $NH_3 \cdot H_2O$) twice and 40 μL loading buffer (10% $NH_3 \cdot H_2O$) twice. The phosphopeptides were resuspended in 40 μL loading buffer and loaded onto the Stage-Tip. Then the phosphopeptides were eluted in a sequential gradient of ACN (0% ACN, 2% ACN, 5% ACN, 8% ACN, 10% ACN, 20% ACN, 40% ACN, 50% ACN, 80% ACN) in 10% $NH_3 \cdot H_2O$ buffer (20 μL/fraction). All the 9 fractions were combined to 3 fractions (0% ACN, 8% ACN, 40% ACN for fraction 1; 2% ACN, 10% ACN, 50% ACN for fraction 2; 5% ACN, 20% ACN, 80% ACN for fraction 3). All of these 3 fractions were lyophilized immediately.

4.4 LC-MS/MS Analysis and Database Search

The fractionated enriched peptides were eluted on a Thermo Fisher EASY-nLC 1200 liquid chromatography and analyzed by Orbitrap Fusion Lumos Tribrid MS (Thermo Fisher Scientific). Peptides were separated on a 16 cm column with a 75 μm inner diameter packed with Dr. Maisch GmbH reversed-phase material Reprosil-Pur 120 C18-AQ, 1.9 μm resin (SinoAmerican Proteomics, LLC). Separation was performed using 75 min runs at a flow rate of 300 nL/min through nonlinear gradient. The elution gradient was as follows: 3-10% B for 3 min, 10-24% B for 55 min, 24-32% B for 10 min, 32-90% B for 4 min, and 90% B for 3 min (Phase A: 0.1% FA and 2% ACN in ddH_2O; Phase B: 0.1% FA in 80% ACN). The initial MS spectrum (MS1) was analyzed over a range of m/z 350-1500 with a resolution of 60,000 at m/z 400. The automatic gain control (AGC) was set as 4×10^5. The subsequent MS spectrum (MS2) was analyzed using data-dependent mode searching for the top 40 intense ions fragmented in the linear ion trap via high-energy collision dissociation (HCD) with the NCE set at 30. The MS2 resolution was 15,000 at m/z 400. The cycle time was 4s.

MS/MS raw files were processed in MaxQuant (version 1.5.3.8) against the uniprot Mus musculus database (downloaded at 2018.04.10, containing 16,972 sequences) for peptide identification, label-free

quantification, and phosphosite localization. The parameters set for database searching were as follows: cysteine carbamidomethyl was specified as a fixed modification. Oxidation of methionine, phospho (STY) and protein N-acetylation and were set as variable modifications. The tolerances of precursor and fragment ions were set at 20 ppm. For digestion, trypsin was set as protease with utmost two missed cleavage permitted. False discovery rate was set as 1% at protein, peptide and modification level. Matched between runs and label free quantification were selected.

4.5 Data management

Proteins/peptides in the reverse decoy database and potential contaminant database were excluded. The localization probability of phosphorylation ranged from 0 to 1, and peptides with localization probabilities of > 0.75 were grouped into Class I and were selected for further analysis. Normalization was performed with Perseus (v.1.6.5.0) [15] by dividing the intensity by the median of each group. Using a two-sample *t*-test, a site with p-value < 0.05 was considered as differentially expressed. Upregulated and downregulated sites were determined as fold-change (FC, mean values of old mice/mean values of young mice) > 1 or < 1, respectively.

4.6 Functional enrichment analysis

Kyoto Encyclopedia of Genes and Genomes (KEGG) [16] enrichment analysis was performed using KOBAS [17]. We chose hypergeometric test/Fisher's exact test as the statistical method and QVALUE as the FDR correction method. KEGG terms with a corrected p-value of < 0.05 were considered as significantly enriched

4.7 Motif analysis

Phosphorylated peptides were submitted to MoMo modification motifs (http://meme-suite.org/tools/momo) [18] to get the sequence characteristics using the motif-x algorithm.

4.8 Kinase prediction and kinase-substrate interaction analysis

All the identified phosphosites were uploaded to NetworKIN [19] for kinase prediction following the algorithm's instructions. Based on the Gene Set Enrichment Analysis (GSEA) principle [20], kinase activity were calculated and matched to the human kinome tree. Kinome tree modified courtesy of Cell Signalling Technology Inc. (www.cellsignal.com) and annotated using Kinome Render [21].

For strict kinase-substrate analysis, network among proteins with differentially expressed phosphosites was constructed according to the manually curated PhosphositePlus database [22]. We used the cytoscape software to present the kinase-substrate interactions.

5. Transcriptome and analysis

RNA isolation, library preparation, and sequencing were performed by Novogene Bioinformatics Technology Co., Ltd (Tianjin, China). Briefly, a total of 3 mg RNA per sample was used as input material

for RNA sample preparation. Firstly, ribosomal RNA was removed with the Epicentre Ribo-zero™ rRNA Removal Kit (RZH1046, Epicentre, USA), and rRNA free residue was cleaned up by ethanol precipitation. Subsequently, sequencing libraries were generated using the rRNA-depleted RNA by NEBNext® Ultra™ Directional RNA Library Prep Kit for Illumina® (NEBE7770, NEB, USA) following manufacturer's recommendations. Fragmentation was carried out using divalent cations under elevated temperature in NEBNext First Strand Synthesis Reaction Buffer (5×). First strand cDNA was synthesized using random hexamer primer and M-MuLV Reverse Transcriptase (RNase H). Second strand cDNA synthesis was subsequently performed using DNA Polymerase I and RNase H. In the reaction buffer, dTTP was replaced by dUTP. Remaining overhangs were converted into blunt ends via exonuclease/polymerase activities. After adenylation of 3' ends of DNA fragments, NEBNext Adapter with hairpin loop structure was ligated to prepare for hybridization. To select cDNA fragments of preferentially 150~200 bp in length, library fragments were purified with AMPure XP system (Beckman Coulter, Beverly, USA). Next, 3 mL USER Enzyme (NEB, USA) was used with size-selected, adaptor-ligated cDNA at 37 °C for 15 min followed by 5 min at 95 °C before PCR. PCR was performed with Phusion High-Fidelity DNA polymerase, Universal PCR primers, and Index (X) Primer. At last, products were purified (AMPure XP system) and library quality was assessed on an Agilent Bioanalyzer 2100 system. Clustering of the index-coded samples was performed on a cBot Cluster Generation System using TruSeq PE Cluster Kit v3-cBot-HS (Illumina) according to the manufacturer's instructions. After cluster generation, the libraries were sequenced on an Illumina HiSeq 4000 instrument, and 150 base pair and paired-end reads were generated. For quality control, raw data in fastq format were first processed using Novogene Perl scripts. Clean data were obtained by removing reads containing adapters, reads containing poly-N, and low-quality reads from the raw data. In addition, the Q20, Q30, and GC contents of the clean data were calculated. All down-stream analyses were based on the clean data with high quality. RNA sequencing data were deposited in the Sequence Read Archive under the BioProject ID PRJNA609589.

Reference genome and gene model annotation files were downloaded from the Ensembl website (genome: ftp://ftp.ensembl.org/pub/release-97/fasta/mus_musculus/dna/Mus_musculus.GRCm38.dna.primary_assembly.fa.gz; gtf: ftp://ftp.ensembl.org/pub/release-97/gtf/mus_musculus/Mus_musculus.GRCm38.97.gtf.gz). HISAT2 (v2.0.5) was used to build the reference genome index and align paired-end clean reads to the reference genome. Then, StringTie (v1.3.3) was used to assemble the mapped reads of each sample and calculate FPKMs of coding genes. FPKM means fragments per kilo-base of exon per million fragments mapped, calculated based on the length of the fragments and reads count mapped to this fragment. Transcripts with FPKM values > 1 in over 50% of the samples in either group were considered validated. The edgeR R package (v3.243) provided statistical routines for determining differential expression in digital transcript or gene expression data using a model based on a negative binomial distribution. Transcripts with adjusted p-values < 0.05 were considered to be differentially expressed. Up- and down-regulated transcripts were determined based on the log2 fold-change (FC, generated by edgeR, mean values of old mice/mean values of young mice) > 0 or < 0, respectively.

6. Transcription factor (TF)-target interaction analysis

TRRUST collects 6,552 TF-target interactions for 828 mouse TFs [23]. According to the trust_rawdata.mouse.tsv file downloaded on 2021/01/08, we selected TFs from phosphoproteome-identified proteins with differentially expressed phosphosites and targets from transcriptome-identified differentially expressed transcripts. TF-target interaction network was constructed by the Cytoscape software.

Results

1. General condition of young and old mice and workflow of phosphoproteome analysis.

Fourteen 2-month-old young and ten 18-month-old aged mice were euthanized in this study. Old mice weighted 32.72 ± 1.937 g, significantly heavier than young ones (25.79 ± 0.482 g; Fig. S1A). The liver index (liver weight/body weight) of old mice was 5.055 ± 0.2444%, slightly higher than that of young (4.459 ± 0.1218%; Fig. 1A). Oil Red O staining showed a clear fat accumulation in old livers but not in young ones (Fig. 1B), consistent with a previous report [24]. However, H & E and Masson staining showed no obvious differences between livers of young and old mice (Fig. S1B).

For phosphoproteome analysis, livers were collected from young and old mice and rapidly frozen. Case by case trypsin digestion and Ti^{4+}-IMAC enrichment for phosphopeptides were processed using each tissue homogenate. Phosphopeptides per mouse were then separated into 3 fractions and measured in a high-resolution quadrupole-Orbitrap MS. Raw MS files were analyzed by MaxQuant for peptide identification, label-free quantification, and phosphosite localization (Fig. 1C).

2. Global phosphoproteome profiling of livers in young and old mice.

We checked identified spectra and peptides for phosphorylated proteins (Fig. S2A), peptide length (Fig. S2B), mass error (Fig. S2C), and Andromeda score distribution (Fig. S2D) for quality control. After exclusion of potential contaminant and reverse peptides, 17,424 unique phosphopeptides corresponding to 14,649 unique phosphosites were matched to 3,736 proteins (Fig. S2A). We kept 10,091 sites, whose localization probabilities were > 0.75, for quantitative filtration (Fig. S2E). Finally, 5,685 phosphosites, quantified in at least 50% of young mice or old ones (Table S1), were used for statistical analysis.

Principle component analysis (PCA) showed that the overall phosphorylation state of livers from old mice was to some extent distinguished from young ones (Fig. 2A). Using a two-sample *t* test, we identified 923 phosphosites in 633 proteins that were statistically significantly regulated during aging, including 430 upregulated sites and 493 downregulated ones (Table S2). The differences of each phosphosite between the means of old and young mice was plotted with the corresponding *P*-value in Fig. 2B. We uploaded phosphorylated proteins to Ingenuity Pathway Analysis for protein localization and type analysis. Compared to proteins with downregulated phosphosites, proteins with upregulated ones more frequently

located at cytoplasm but less at nucleus (Fig. 2C), and they contained increased proportion of enzymes, kinases, and transporters but decreased transcription regulators (Fig. 2D).

3. Integration of altered pathways in mouse liver during normal aging.

To comprehensively find out the phosphorylation-regulated pathways, we performed a three-step pathway construction. Firstly, we uploaded all the identified phosphosites to NetworKIN [25] for kinase prediction following the algorithm's instructions. Based on the Gene Set Enrichment Analysis (GSEA) principle [26], we got the putative activity of each predicted kinase, finding activated Mkk6/Map2k6, Pkab, Pkca, Ampka1, and Nek1, and repressive Tgfbr2, Mek1/Map2k1, Mek2/Map2k2, Rsk3, p70s6k, Cdk7, Clk1, and Clk2 (Fig. 3A). Previous report shows that XpSPX motif is likely to be phosphorylated by mitogen-activated protein kinases (Mapks) while RXXpS and RSXpS by Pkcs and Pkas [27, 28]. We utilized the Motif-X algorithm to get the featured motifs of up and down phosphosites, but found predicted kinase activity and actually identified motifs did not exactly match (Fig. S2F). We therefore used PhosphositePlus, the continuously updated database containing manually curated kinase-substrate interactions [28], for a second step of pathway construction. Among the proteins containing differentially regulated phosphosites, we observed a concise kinase-substrate network, including Egfr-Mapk1, Prkaa2 (Ampk2)-Acaca, etc. (Fig. 3B). Then for step three, we did KEGG enrichment analysis using proteins with upregulated and downregulated phosphosites. We found aging-associated increase of phosphorylation was related to metabolism and secretion (Fig. 3C) and decreased phosphorylation was to cancer, which is characterized by abnormal cell cycle/proliferation (Fig. 3D). Finally, combined with the above three-step analysis, we constructed a phosphorylation-associated signaling network in mouse liver during aging (Fig. 4). Among the proteins with upregulated phosphosites, we observed fatty acid biosynthesis, b-oxidation, and potential Ca^{2+}-associated secretory process. As for proteins with downregulated phosphosites, we saw Egfr-Sos1-Araf/Braf-Map2k1-Mapk1 and potential Ctnnb1 pathway, both related to cell survival and proliferation [29-31].

4. Potential extended transcription factor-target relationships between phosphoproteome and transcriptome in mouse liver during normal aging.

We also tried to link phosphorylation with other important regulatory elements, such as transcription factors (TFs). We did transcriptome analysis for livers from 8 young mice and 9 old ones and identified 13,275 transcripts (brief quality control metrics in Table S3 and Table S4). Same as previous report, the transcriptome distinguished livers from young and old mice [32], which was confirmed by hierarchical clustering (Fig. S3A) and PCA (Fig. S3B). FC and adjusted *P*-value of each transcript were calculated using the edgeR R package and plotted in Fig. S3C. The differentially expressed transcripts (813 upregulated and 629 downregulated ones) were enriched for metabolic pathways but fatty metabolism was not prominent (Fig. S3D, S3E). TRRUST collects 6,552 TF-target interactions for 828 mouse TFs [33]. Based on TRRUST, 10 proteins with differentially expressed phosphosites in the phosphoproteome were identified as TFs (e.g. Hnf4a and Ctnnb1) and they had 20 corresponding downstream transcripts in the transcriptome (Fig. S4). We saw Ctnnb1 and Hnf4a widely associated with multiple transcripts (low

phosphorylation of Ctnnb1 associated with increased transcription of Tbx3, Cyp2b10, Pdgfra, and Axin2 and decreased transcription of Foxa2, Vegfa, Grem2, and Cdh1; high phosphorylation of Hnf4a associated with increased transcription of Apoa4 and Cyp2b9 and decreased transcription of Foxa1, Foxa2, Onecut1, Cyp4a12b, Cyp3a11, and Gstp1). Low phosphorylation of Ybx1 was related to decreased transcription of Egfr and high phosphorylation of Gtf2i was related to increased transcription of Tgfbr2. We calculated Pearson correlation coefficients between phosphosites and transcripts (Table S5). Though complex, our research provided some clues for potential relationships between phosphorylated TFs and their downstream transcripts.

Discussion

In this study, we performed LC-MS based phosphoproteome analysis with livers of fourteen 2-month-old and ten 18-month-old mice. We constructed a phosphorylation-associated signaling network in mouse liver during aging, showing increased phosphorylation of proteins in fatty acid biosynthesis, β-oxidation, and potential Ca^{2+}-associated secretory process, together with decreased phosphorylation of Egfr-Sos1-Araf/Braf-Map2k1-Mapk1 and potential Ctnnb1 pathway.

Previous report has revealed cellular senescence, a permanent cell cycle arrest state accompanied with secretory phenotype, exacerbates aging [2]. Elimination of senescent cells has presented promising therapeutic effects on aging-associated disorders [34], including hepatic steatosis [24]. Besides previously reported increased p16(Ink4a) [35], our study suggested low phosphorylation of Egfr, Mapk, and Ctnnb1, which were related to cell survival and proliferation [29–31], might promote senescence and might be targets for aging intervention.

Besides the general metabolism and inflammation process identified by previous aging-associated transcriptome and proteome research [8, 36, 37], phosphoproteome seemed to provide a distinctive profile of aging, presenting potentially dysregulated fatty acid metabolism, secretory process, and cells cycle/proliferation. Consulting the report that sorafenib activates AMPK and ameliorates nonalcoholic steatohepatitis [38], we think intervention of phosphorylation state or kinase activity may provide novel ways to ameliorate aging.

Furthermore, there are some issues deserves further discussion. Firstly, though most phosphosites in the constructed phosphorylated network have been recorded in PhosphositePlus, evidences mostly came from MS experiment. Functional experiments based exploration are still needed for phosphosites annotation. Secondly, we did not analyze aging-associated proteome because different batches of MS data are quite independent. However, further multi-omics integration with advanced technologies may provide much more abundant information for data mining. Thirdly, 24 male mice were euthanized by tribromoethanol but the influence of gender and anesthetics on this experimental system was difficult to assess in this study. It is important to investigate other organs and both sexes in future studies to avoid biases [39] and to obtain a comprehensive profile of liver aging and systematic aging.

Overall, our study obtained the first phosphoproteome profiling of mouse livers using LC-MS/MS during normal aging. Global view of tissues with advanced omics technology may help us find integrated mechanism of aging then find potential intervention methods.

Conclusions

In summary, we constructed a phosphorylation-associated network in the liver of mice during normal aging, which may help to discover novel anti-aging strategies.

Declarations

Ethics approval and consent to participate

This study was approved by the Laboratory Animal Management and Ethics Committee of Institute of Basic Medical Sciences, Chinese Academy of Medical Sciences.

Consent for publication

Not applicable

Availability of data and materials

Raw phosphoproteome data are deposited in the ProteomeXchange Consortium under the identifier PXD024270. Raw transcriptome data are deposited in the Sequence Read Archive under the ID PRJNA609589.

Competing interests

The authors declare that they have no competing interests.

Funding

This work was supported by grants from the Chinese Academy of Medical Sciences Innovation Fund for Medical Sciences (CIFMS2017-I2M-1-008, CIFMS2019-I2M-1-004).

Authors' contributions

J.Y. conceived and designed the project. P.X. did phosphoproteome MS experiments. J.L., S.W., Y.Y., and S.L. performed the analysis. J.L., J.Y., S.W. and Y.W. wrote the paper. All authors reviewed and approved the manuscript.

Acknowledgements

Not applicable

References

1. Partridge L, Deelen J, Slagboom PE. Facing up to the global challenges of ageing. Nature. 2018;561:45–56.
2. Lopez-Otin C, Blasco MA, Partridge L, Serrano M, Kroemer G. The hallmarks of aging. Cell. 2013;153:1194–217.
3. Campisi J, Kapahi P, Lithgow GJ, Melov S, Newman JC, Verdin E. From discoveries in ageing research to therapeutics for healthy ageing. Nature. 2019;571:183–92.
4. Rivero-Segura NA, Bello-Chavolla OY, Barrera-Vazquez OS, Gutierrez-Robledo LM, Gomez-Verjan JC. Promising biomarkers of human aging: In search of a multi-omics panel to understand the aging process from a multidimensional perspective. Ageing Res Rev. 2020;64:101164.
5. Morsiani C, Bacalini MG, Santoro A, Garagnani P, Collura S, D'Errico A, et al. The peculiar aging of human liver: A geroscience perspective within transplant context. Ageing Res Rev. 2019;51:24–34.
6. Horvath S, Erhart W, Brosch M, Ammerpohl O, von Schonfels W, Ahrens M, et al. Obesity accelerates epigenetic aging of human liver. Proc Natl Acad Sci U S A. 2014;111:15538–43.
7. Benayoun BA, Pollina EA, Singh PP, Mahmoudi S, Harel I, Casey KM, et al. Remodeling of epigenome and transcriptome landscapes with aging in mice reveals widespread induction of inflammatory responses. Genome Res. 2019;29:697–709.
8. Kim Y, Kwon OK, Chae S, Jung HJ, Ahn S, Jeon JM, et al., Quantitative Proteomic Analysis of Changes Related to Age and Calorie Restriction in Rat Liver Tissue, Proteomics 2018;18:e1700240.
9. Sato S, Solanas G, Peixoto FO, Bee L, Symeonidi A, Schmidt MS, et al., Circadian Reprogramming in the Liver Identifies Metabolic Pathways of Aging, Cell 2017;170:664-677 e611.
10. Robles MS, Humphrey SJ, Mann M. Phosphorylation Is a Central Mechanism for Circadian Control of Metabolism and Physiology. Cell Metab. 2017;25:118–27.
11. Wattacheril J, Rose KL, Hill S, Lanciault C, Murray CR, Washington K, et al. Non-alcoholic fatty liver disease phosphoproteomics: A functional piece of the precision puzzle. Hepatol Res. 2017;47:1469–83.
12. Tian M, Cheng H, Wang Z, Su N, Liu Z, Sun C, et al. Phosphoproteomic analysis of the highly-metastatic hepatocellular carcinoma cell line, MHCC97-H. Int J Mol Sci. 2015;16:4209–25.
13. Zhou H, Ye M, Dong J, Corradini E, Cristobal A, Heck AJ, et al. Robust phosphoproteome enrichment using monodisperse microsphere-based immobilized titanium (IV) ion affinity chromatography. Nat Protoc. 2013;8:461–80.
14. Rappsilber J, Mann M, Ishihama Y. Protocol for micro-purification, enrichment, pre-fractionation and storage of peptides for proteomics using StageTips. Nat Protoc. 2007;2:1896–906.
15. Tyanova S, Temu T, Sinitcyn P, Carlson A, Hein MY, Geiger T, et al. The Perseus computational platform for comprehensive analysis of (prote)omics data. Nat Methods. 2016;13:731–40.
16. Kanehisa M, Araki M, Goto S, Hattori M, Hirakawa M, Itoh M, et al. KEGG for linking genomes to life and the environment. Nucleic Acids Res. 2008;36:D480–4.

17. Xie C, Mao X, Huang J, Ding Y, Wu J, Dong S, et al. KOBAS 2.0: a web server for annotation and identification of enriched pathways and diseases. Nucleic Acids Res. 2011;39:W316–22.
18. Cheng A, Grant CE, Noble WS, Bailey TL. MoMo: discovery of statistically significant post-translational modification motifs. Bioinformatics. 2018;35:2774–82.
19. Horn H, Schoof EM, Kim J, Robin X, Miller ML, Diella F, et al. KinomeXplorer: an integrated platform for kinome biology studies. Nat Methods. 2014;11:603–4.
20. Subramanian A, Tamayo P, Mootha VK, Mukherjee S, Ebert BL, Gillette MA, et al. Gene set enrichment analysis: a knowledge-based approach for interpreting genome-wide expression profiles. Proc Natl Acad Sci U S A. 2005;102:15545–50.
21. Chartier M, Chenard T, Barker J, Najmanovich R. Kinome Render: a stand-alone and web-accessible tool to annotate the human protein kinome tree. PeerJ. 2013;1:e126.
22. Hornbeck PV, Zhang B, Murray B, Kornhauser JM, Latham V, Skrzypek E. PhosphoSitePlus, 2014: mutations, PTMs and recalibrations. Nucleic Acids Res. 2015;43:D512–20.
23. Han H, Cho JW, Lee S, Yun A, Kim H, Bae D, et al. TRRUST v2: an expanded reference database of human and mouse transcriptional regulatory interactions. Nucleic Acids Res. 2018;46:D380–6.
24. Ogrodnik M, Miwa S, Tchkonia T, Tiniakos D, Wilson CL, Lahat A, et al. Cellular senescence drives age-dependent hepatic steatosis. Nat Commun. 2017;8:15691.
25. Horn H, Schoof EM, Kim J, Robin X, Miller ML, Diella F, et al. KinomeXplorer: an integrated platform for kinome biology studies. Nat Methods. 2014;11:603–4.
26. Subramanian A, Tamayo P, Mootha VK, Mukherjee S, Ebert BL, Gillette MA, et al. Gene set enrichment analysis: a knowledge-based approach for interpreting genome-wide expression profiles. Proc Natl Acad Sci U S A. 2005;102:15545–50.
27. Ren L, Li C, Wang Y, Teng Y, Sun H, Xing B, et al. In Vivo Phosphoproteome Analysis Reveals Kinome Reprogramming in Hepatocellular Carcinoma. Mol Cell Proteomics. 2018;17:1067–83.
28. Hornbeck PV, Zhang B, Murray B, Kornhauser JM, Latham V, Skrzypek E. PhosphoSitePlus, 2014: mutations, PTMs and recalibrations. Nucleic Acids Res. 2015;43:D512–20.
29. Johnson AA, Shokhirev MN, Wyss-Coray T, Lehallier B. Systematic review and analysis of human proteomics aging studies unveils a novel proteomic aging clock and identifies key processes that change with age. Ageing Res Rev. 2020;60:101070.
30. Park JW, Ji YI, Choi YH, Kang MY, Jung E, Cho SY, et al. Candidate gene polymorphisms for diabetes mellitus, cardiovascular disease and cancer are associated with longevity in Koreans. Exp Mol Med. 2009;41:772–81.
31. Tornesello ML, Buonaguro L, Tatangelo F, Botti G, Izzo F, Buonaguro FM. Mutations in TP53, CTNNB1 and PIK3CA genes in hepatocellular carcinoma associated with hepatitis B and hepatitis C virus infections. Genomics. 2013;102:74–83.
32. White RR, Milholland B, MacRae SL, Lin M, Zheng D, Vijg J. Comprehensive transcriptional landscape of aging mouse liver. BMC Genom. 2015;16:899.

33. Han H, Cho JW, Lee S, Yun A, Kim H, Bae D, et al. TRRUST v2: an expanded reference database of human and mouse transcriptional regulatory interactions. Nucleic Acids Res. 2018;46:D380–6.
34. Xu M, Pirtskhalava T, Farr JN, Weigand BM, Palmer AK, Weivoda MM, et al. Senolytics improve physical function and increase lifespan in old age. Nat Med. 2018;24:1246–56.
35. Baker DJ, Childs BG, Durik M, Wijers ME, Sieben CJ, Zhong J, et al. Naturally occurring p16(Ink4a)-positive cells shorten healthy lifespan. Nature. 2016;530:184–9.
36. Srivastava A, Barth E, Ermolaeva MA, Guenther M, Frahm C, Marz M, Witte OW. Tissue-specific Gene Expression Changes Are Associated with Aging in Mice. Genomics Proteomics Bioinformatics; 2020.
37. Moaddel R, Ubaida-Mohien C, Tanaka T, Lyashkov A, Basisty N, Schilling B, et al., Proteomics in aging research: A roadmap to clinical, translational research, Aging Cell 2021;e13325.
38. Jian C, Fu J, Cheng X, Shen LJ, Ji YX, Wang X, et al., Low-Dose Sorafenib Acts as a Mitochondrial Uncoupler and Ameliorates Nonalcoholic Steatohepatitis, Cell Metab 2020;31:892–908 e811.
39. Mitchell SJ, Madrigal-Matute J, Scheibye-Knudsen M, Fang E, Aon M, Gonzalez-Reyes JA, et al. Effects of Sex, Strain, and Energy Intake on Hallmarks of Aging in Mice. Cell Metab. 2016;23:1093–112.

Figures

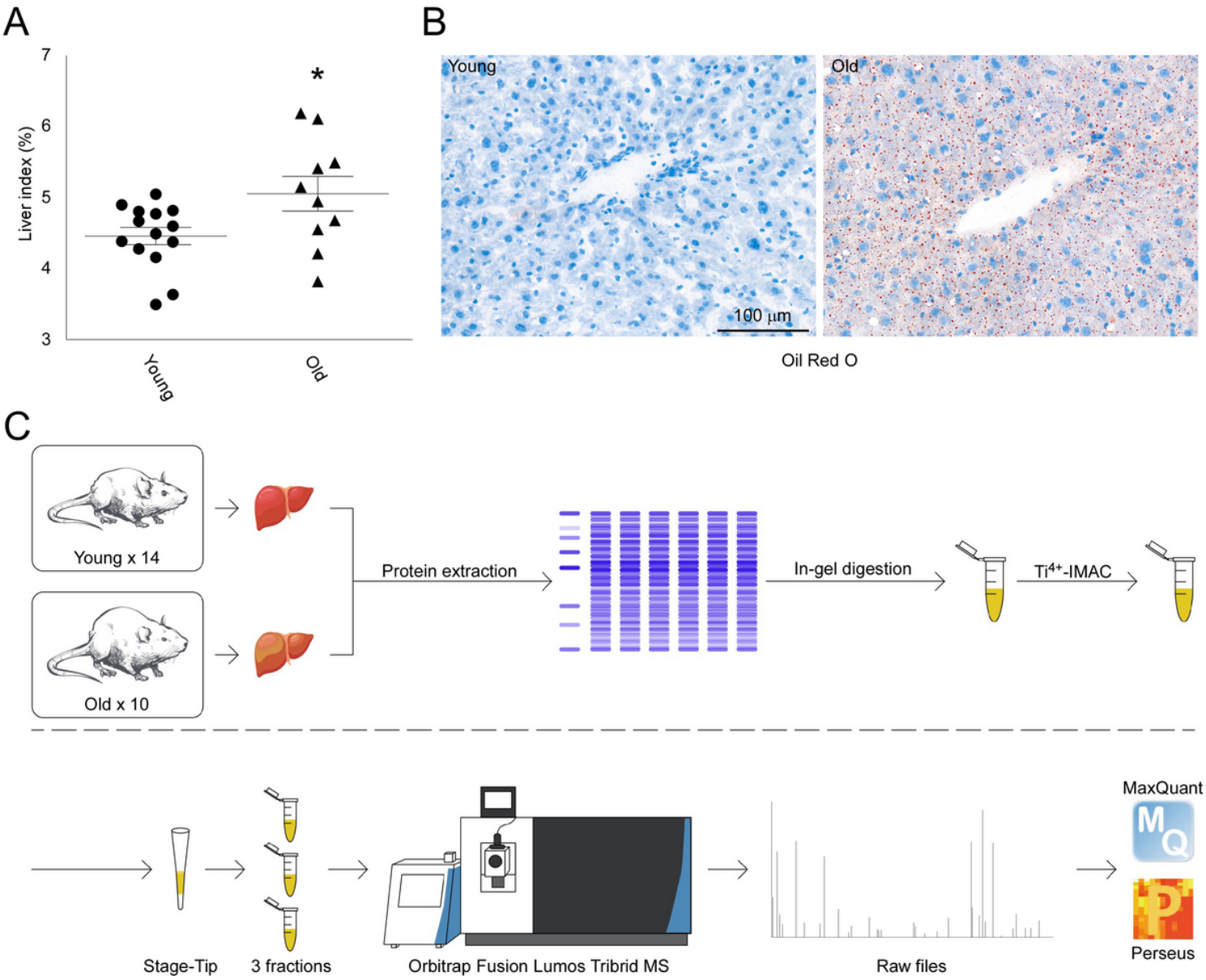

Figure 1

General description of mouse liver during normal aging and workflow of the phosphoproteome detection process. (A) Liver index of mice (young: n = 14; old: n = 10; mean ± standard error of the mean shown; *t test, $p < 0.05$). (B) Oil red O staining of young and old mouse livers. (C) Workflow of the phosphoprotome detection process.

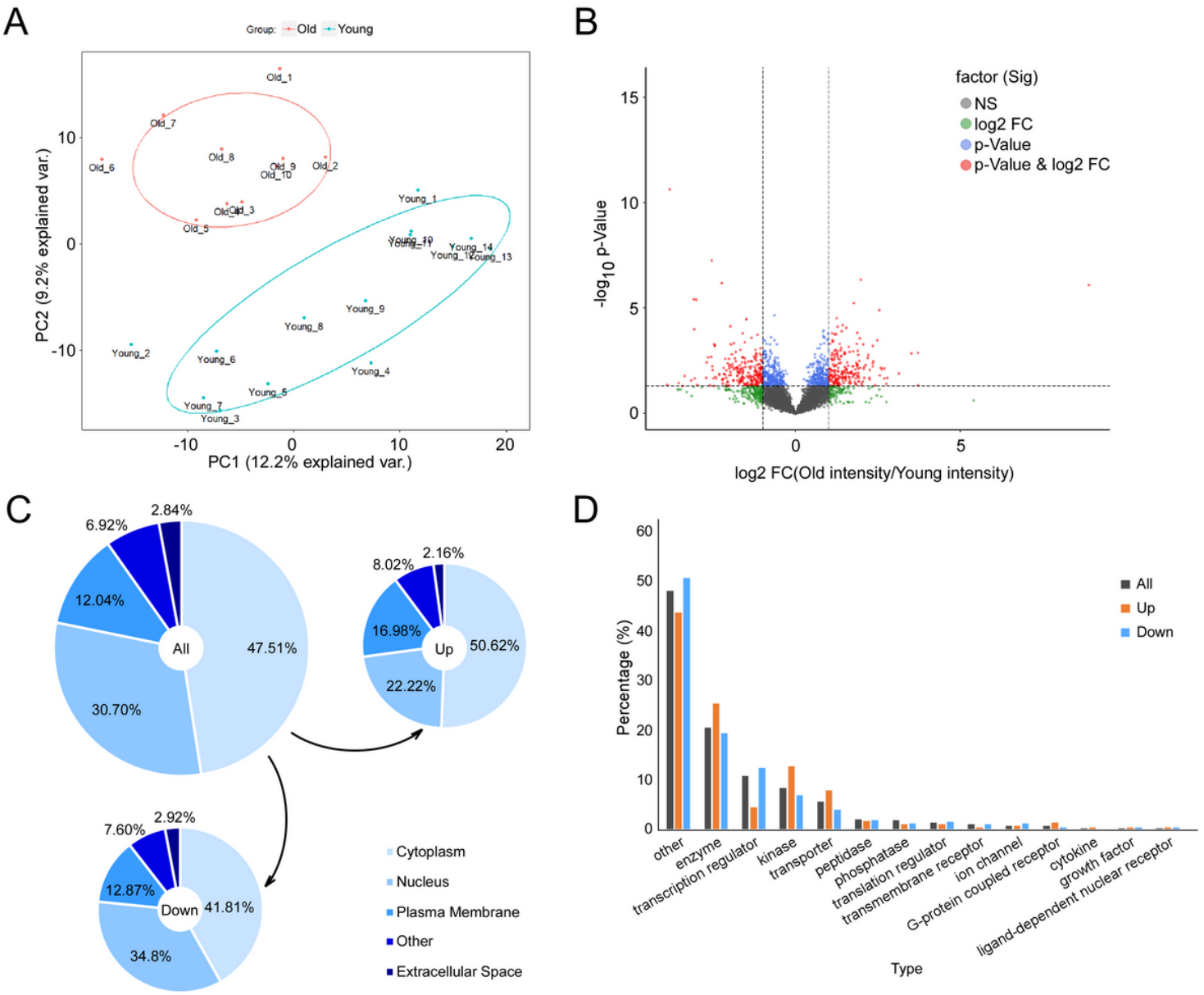

Figure 2

Global phosphoproteome profiling of livers in young and old mice. (A) PCA of filtered phosphosites in livers of young and old mice. (B) FC and P-value (two-sample t test) of each filtered phosphosite were plotted in a volcano plot. (C) Proteins with phosphosites were submitted to Ingenuity Pathway Analysis (IPA) for location prediction. Total: proteins corresponding to the filtered 5,685 sites. Up: proteins corresponding to the 430 upregulated sites. Down: proteins corresponding to the 493 downregulated sites. (D) Proteins with phosphosites were submitted to IPA for type prediction. Total: proteins corresponding to the filtered 5,685 sites. Up: proteins corresponding to the 430 upregulated sites. Down: proteins corresponding to the 493 downregulated sites.

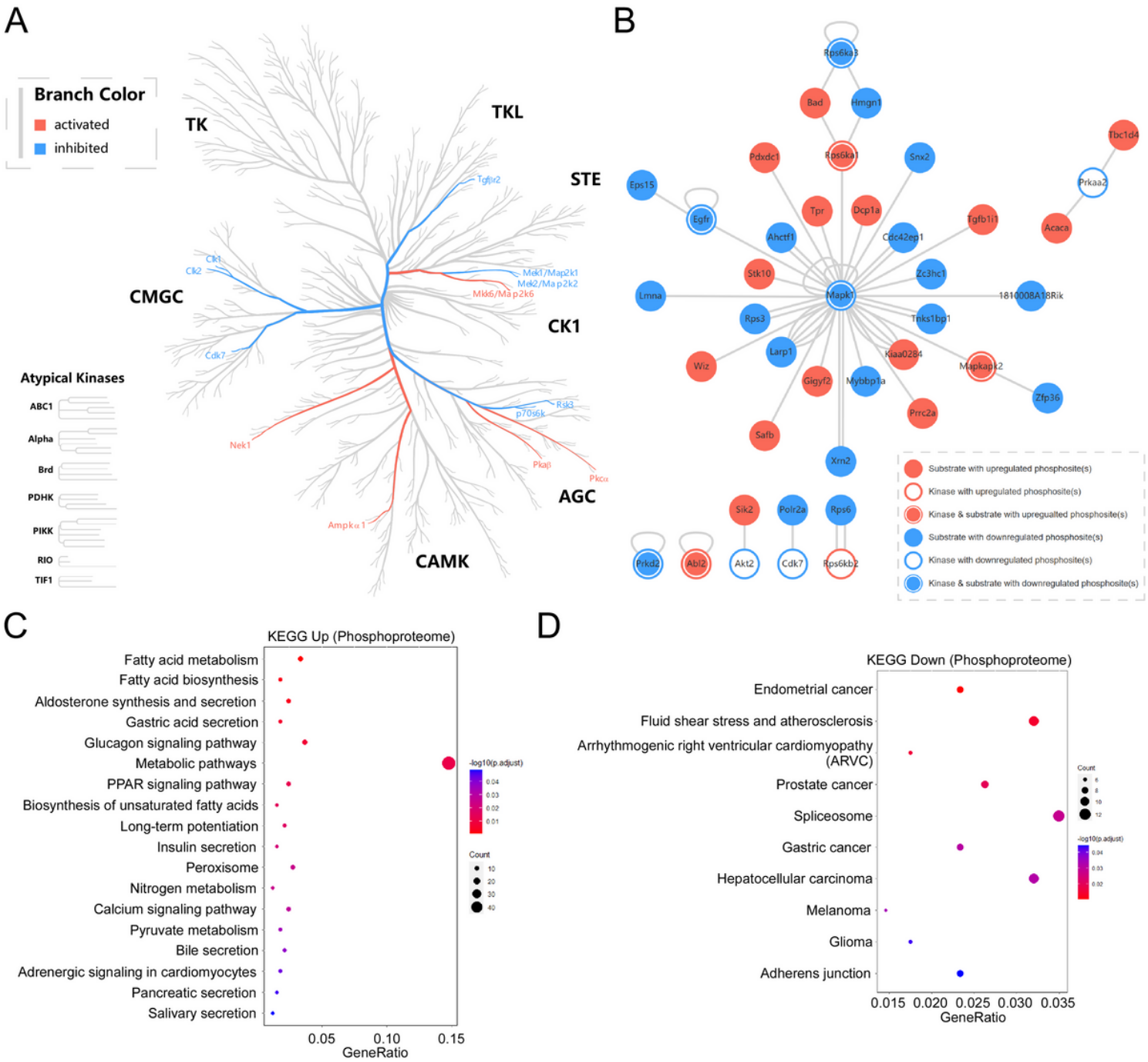

Figure 3

Phosphorylation-associated pathway construction in mouse liver during aging. (A) Predicted kinase activity based on NetworKIN were mapped to human kinome tree. (B) Kinase-substrate interactions among the proteins with differentially expressed phosphosites were constructed based on PhosphositePlus using the Cytoscape software. (C) Enriched KEGG pathways for proteins with upregulated phosphosites. (D) Enriched KEGG pathways for proteins with downregulated phosphosites.

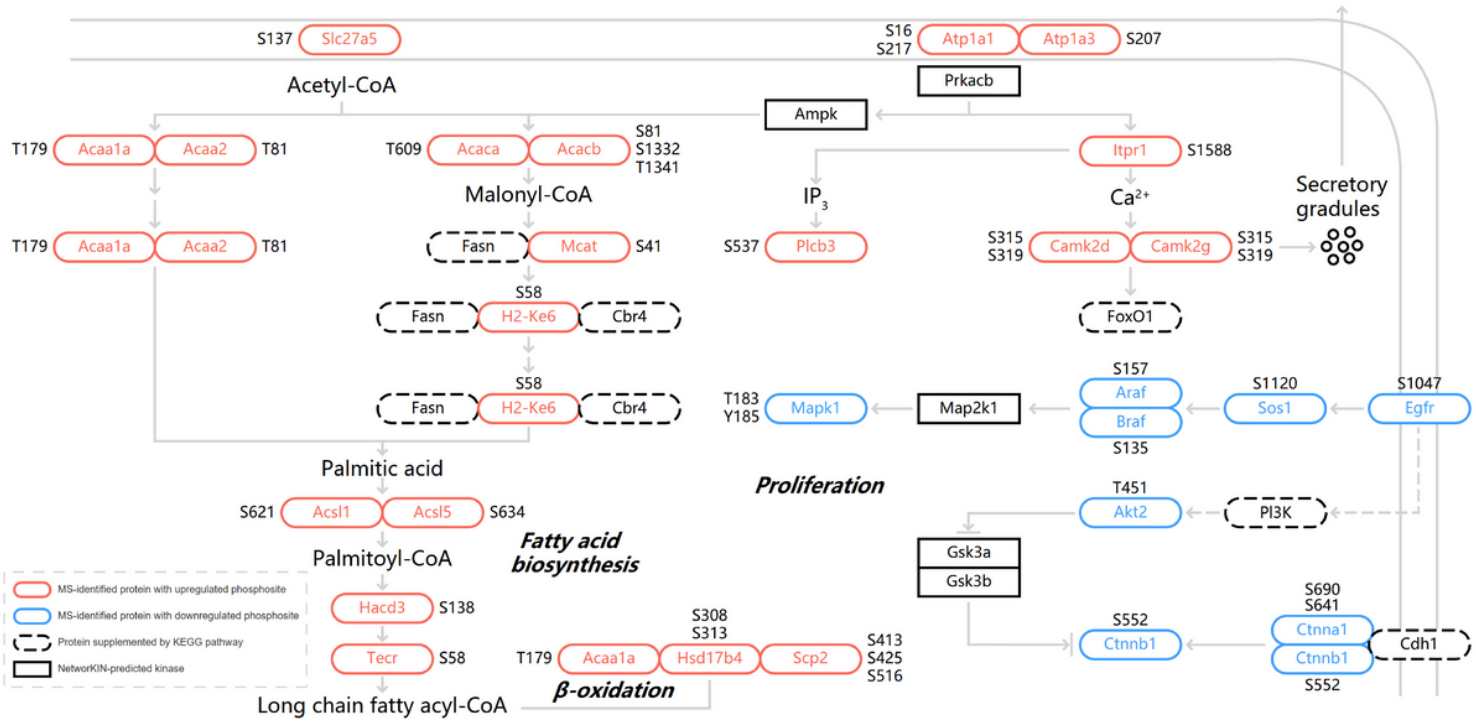

Figure 4

Integrated alteration of pathways in the liver of mice during normal aging. Phosphorylation-associated signaling pathways among proteins with differentially expressed phosphosites based on NetworKIN, PhosphositePlus, and KEGG. Identified phosphosites were annotated next to the proteins.

Supplementary Files

This is a list of supplementary files associated with this preprint. Click to download.

- FigS1general.tif
- FigS2phospho.tif
- FigS3trans.tif
- FigS4phosphoTFtranscripts.tif
- TableS1Quantified5685phosphosites.xlsx
- TableS2Differentiallyexpressed923phosphosites.xlsx
- TableS3Qualitycontrolmetricsfortranscriptome.xlsx
- TableS4Quantified13275transcripts.xlsx
- TableS5TFtargetinteractionsbasedonTRRUST.xlsx